An Experimental Investigation into the Bond-Slip Behaviour between CFRP Composite and Lightweight Concrete

Mustafa Hameed Al-Allaf, Laurence Weekes, Levingshan Augusthus-Nelson and Philip Leach

School of Computing Science and Engineering, University of Salford

Salford, M5 4WT, United Kingdom

ABSTRACT

Epoxy bonded fibre reinforced polymer (FRP) composites are widely used for the retrofit of ailing reinforced concrete structures, for both shear and flexure. The behaviour of retrofitted concrete structures is governed by the bond strength and the material characteristics of the epoxy bonded FRP and the concrete. Previous studies show that lightweight concrete (LWC), which uses Pulverised Fuel Ash (Lytag) instead of coarse granite aggregates, has significantly lower tensile strength and aggregate interlock compared to normal weight concrete. Performance of shear retrofitted concrete elements is primarily governed by the aggregate interlock and tensile strength. Thus the study of FRP enhancement techniques in LWC is paramount for limit state design. Many studies have been conducted to understand the bond-slip behaviour between normal weight concrete (NWC) and FRP composites, where the increasing interfacial (shear) and normal stresses with increasing plastic deformation lead to FRP debonding and/or FRP rupture failures. This paper presents the experimental pull-off test results obtained from lightweight concrete prisms with various configurations of epoxy bonded Carbon FRP (CFRP) sheets. The experimental results show that the LWC can successfully be applied in the strengthening of lightweight concrete structures. However, the lightweight concrete prisms failed due to a diagonal crack within the concrete materials. This was due to a lower tensile strength compared

to normal weight concrete specimens where peeling or rupture of FRP is the dominant failure mechanism.

INTRODUCTION

Structural lightweight concrete (LWC) has become established as an important and versatile material in modern construction. The reasons for development taking place in this field are technical and economic. The use of lightweight concrete has shown that it has many advantages. Its lower density means that the dead weight of the structure can be reduced with a consequent reduction in the size of foundations. Alternatively the dimensions of elements can be considerably enlarged without having to alter erection systems, or the geometric shape of an element can be greatly simplified without increasing its overall weight. Lightweight concrete has been used increasingly over the past decades. In the coming decades it is therefore expected that structures constructed using lightweight concrete will occupy a significant proportion of concrete infrastructures. When deteriorated, these structures may be retrofitted using efficient systems such as FRP reinforcement.

Externally bonded fibre reinforced polymer (FRP) plates or sheets have emerged as a popular method for retrofitting of reinforced concrete (RC) structures **[1]**. This technology offers unique advantages with respect to traditional strengthening techniques. Among those are good immunity to corrosion, lower self-weight and excellent mechanical properties. Furthermore, the hand lay-up allows adaption of FRP reinforcement to the shape of any structural element **[2]**. The performance of the FRP-to-concrete interface in providing an effective stress transfer is of crucial importance **[3]**. Indeed, a number of failure modes in FRP-strengthened RC members are directly caused by debonding of the FRP from the bonded surface. Therefore, the safe and economic design of externally bonded FRP systems needs a sound understanding of the behaviour of FRP-to-concrete interfaces. A significant amount of research has been conducted to investigate the effect of the bond between normal weight concrete and FRP on the failure of adhesively bonded joints. These factors are mainly as follows: concrete compressive or tensile or both strength **[4, 5& 6]**; FRP bonded length **[7&8]**; FRP bonded width [**9&10]**; FRP stiffness **[11&12]**; adhesive properties **[13]**; surface preparation **[14]** and concrete composition **[15]**. However, the study of bond characteristics between lightweight concrete (LWC) substrate and FRP reinforcement has not received much attention. In our experiments, the bonded lengths, width, thickness and fibre orientation of CFRP sheet were varied in order to understand the fracture behaviour and the effectiveness of CFRP on lightweight concrete.

TEST PROGRAMME

The entire experimental program 55 concrete prisms divided into four phases, each phase comprising a different number of samples cast with LWC and NWC bonded with CFRP sheets in eight different CFRP configuration techniques (each technique was repeated in three to four LWC samples and two NWC samples). All specimens of NWC and LWC were cast as the same grade of concrete (i.e. the same compressive strength) to eliminate any unwanted variable in these two types of concrete. The letter ‘’L’’ refers to LWC samples and the letter ’N’’ refers to NWC samples. The details of each series are described as follows:

1. Series (**BN/L1)** contained twenty-one concrete prisms: twelve specimens were cast with LWC and nine specimens were cast with NWC. The specimens were bonded with CFRP sheets of 100mm width and varying lengths of 100, 150 and 200 mm. The main purpose of this series of tests was to determine the bond strength properties, bond-slip behaviour and effective bond length.

2. Series **(BN/L2)** contained twelve concrete prisms: eight prisms were cast with LWC and four specimens were cast with NWC. This series was designed to study the behaviour of CFRP bonded sheets when a pull-out force was inclined to the grain direction of FRP fibre. The angle between the FRP grain fibre and the loading direction was varied at orientation angles of 0^o, 45^o and 90^o.
3. Series **(BN/L3)** contained ten concrete prisms in which six prisms were bonded with LWC and four prisms were cast with NWC. This series examined the effect of using double parallel and perpendicular layers of CFRP sheets.
4. Series **(BN/L4)** contained twelve concrete prisms: eight prisms were cast with LWC and four prisms were cast with NWC. The width of the CFRP sheet (100, 150 and 200 mm) was varied in this series. The main purpose of these tests was to study the effects of the CFRP-to-concrete width ratio.

Double lap shear (DLS) test

Double-lap shear tests on concrete prisms were carried out in order to understand the behaviour of the epoxy bonded CFRP sheet. The nominal dimensions of the prismatic concrete blocks are as follows: length (L = 280 mm), width (b = 200 mm) and height (h = 90 mm). The CFRP sheets were bonded in the centre on both sides of the concrete block. The concrete blocks had been sawn into two separate parts and then re-joined by two threaded rods as shown in Figure 1. In a typical test, the tensile load was applied to the ends of a steel bar, which had been cast inside the concrete block and cut into two parts within the concrete block. In addition, two longitudinal aluminium tubes were provided to facilitate clamping of the sample 'halves' prior to testing. The two threaded rods were released before testing, as shown in Figure 2(c). Also a plastic membrane was placed between the two parts of the concrete block to prevent any undesirable bond from the adhesive entering this interface. In this study, the samples were tested in a 50kN capacity Instron tensile test machine. To negate the effects of any eccentricity causing moment on the sample during testing, a ‘ball and socket’ connection was employed as shown in Figure 2(b). In most of the cases, the maximum slip was less than 2 mm. The displacement of 0.24 mm/min was maintained throughout the test program in order to eliminate the inertial effect of applied load and to capture adequate data over a small period of time (the experiment was expected to last about 1 to 3 mins with the loading rate of 0.24 mm/min). Global slip was measured using two linear voltage displacement transformers (LVDTs), which were set up on both sides of the concrete block as shown in Figure 2(a). To investigate the strain distribution along the length of the CFRP sheet, a series of 3 mm-long strain gauges were attached on the top surface of the CFRP sheets on two samples of (BL/N1-1, BL/N1-2 and BL/N1-3) as shown in Figure 2(d). Strain gauges were installed at shorter distances along the length of CFRP sheet in one part of specimen. The first strain gauge was placed at the centre of the concrete samples and the others were attached along the bond length. The positions of the strain gauges are reported in Table (1).

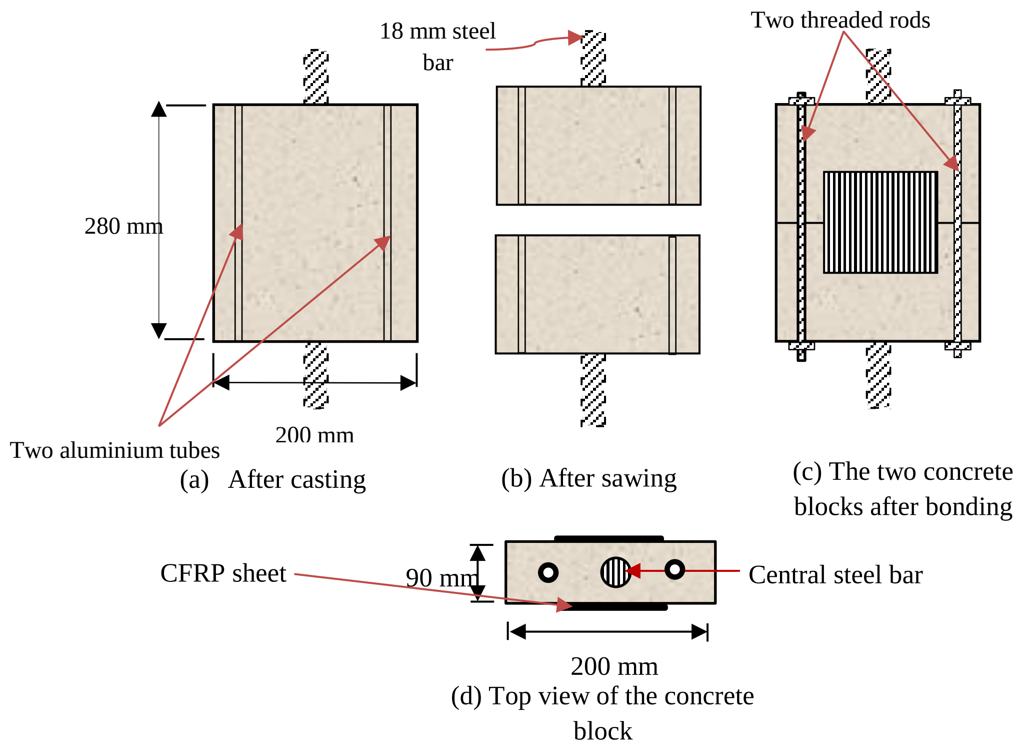

Figure 1: Process of preparing the two concrete blocks for bond testing

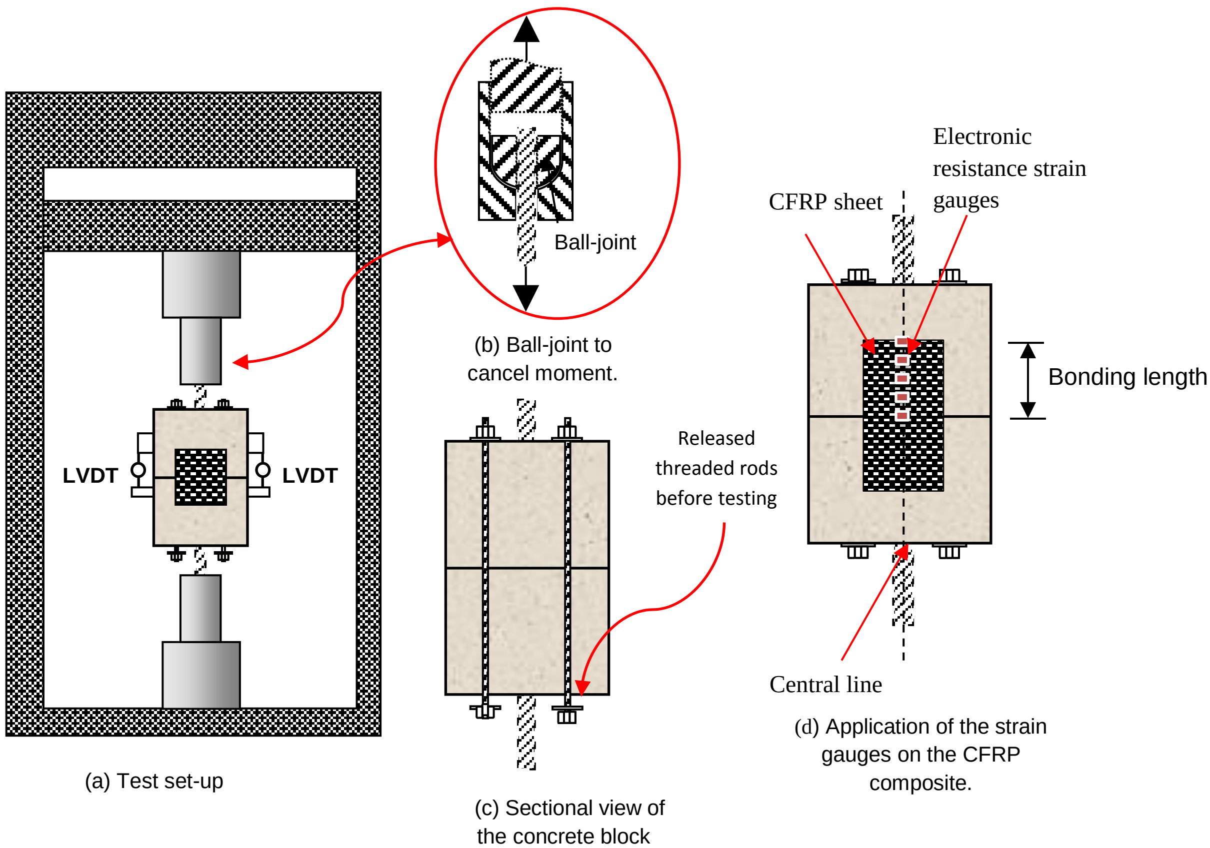

Figure 2: Detail of the double lab test

Table 1: Position of the strain gauges along the length of the CFRP composite

Samples notation	Bonded Length of CFRP sheet (mm)	Distance of the strain gauge from the center of the specimen (mm)								
		SG-1	SG-2	SG-3	SG-4	SG-5	SG-6	SG-7	SG-8	SG-9
BL/N1-1	50	0	10	25	40	50				
BL/N1-2	75	0	10	25	40	50	60	75		
BL/N1-3	100	0	10	25	40	60	70	80	90	100

Material properties

Pulverised Fuel Ash (Lytag) and sand aggregates were used in the preparation of the lightweight concrete mixture. The particle size grading, physical properties and chemical composition of the Lytag aggregates are summarised in Tables 2, 3 and 4 respectively. Coarse granite and sand aggregates were used in preparation of the NWC mixtures. The concrete mixes for both concretes were designed to have a slump of 75 mm, and a 28-day cube compressive strength of 40 N/mm^2. The mix details for the lightweight and normal weight concretes are given in Table 5. A tilting drum mixer was used for mixing the concrete. All the LWC and NWC were cast in a single batch each. In addition, six concrete cubes (100 x 100 x 100 mm), two concrete cylinders (150 dia. x 300 mm) and two prisms (100 x 100 x 400 mm) were cast from each batch to determine the uniaxial compressive strength, the Young's modulus of elasticity and the modulus of rupture of lightweight and normal weight concrete (see Table 6).

Table 2: Particle size distribution of Lytag aggregates

Sieve size (mm)	**Passing %**
14	100%
10	81%
8.0	29%
4.0	4%

Table 3: Physical properties of Lytag aggregates **[16]**

Moisture content as delivered	15%
Long term moisture content	30%
Oven dry loose bulk density	700-800 kg/m^3
Particle density	1300-1650 kg/m^3
Permeability	$1.3x10^{-1}$ m/s

Table 4: Chemical composition of Lytag aggregates **[17]**

SiO_2	53%
Al_2O_3	25%
Fe_2O_3	6%
CaO	4%
Loss on Ignition	3.1%
Chloride	0.01%
Acid Soluble Sulphate	0.1%

Table 5: The mix design of lightweight and normal weight concretes

Concrete Type	Water (kg)	Cement (kg)	Sand (kg)	Coarse Aggregate (kg)	Design Strength N/mm^2
NWC	192	400	667	1184	40
LWC	216*	480	485	715	40

* The moisture content and absorption of lightweight aggregates were considered in calculations of mix design.

Table 6: Mechanical properties of concrete

Concrete Type	Average cube concrete strength f_c' (MPa)	Average modulus of rupture f_r (MPa)	Average modulus of elasticity E_c (MPa)	Average concrete density ρ_c (kg/m^3)
NWC	41.6	3.4	29670	2345
LWC	40.1	2.9	22900	1776
(S.D)	2.40	0.43		

S.D: is the standard deviation.

A unidirectional CFRP sheet with a thickness of 0.117 mm, a tensile strength of 4000 MPa, a Young's modulus of 240 GPA and a strain at failure of 1.6% were used. Epoxy plus primer (EN-

Force primer) and epoxy plus adhesive (EN-Force bonding adhesive) were used to bond the CFRP composite to the concrete substrate respectively. Both primer and adhesive are two-component epoxy based adhesives. Part A of the epoxy is the base component while Part B is the hardener which should be made of approximately 2/3 base and 1/3 hardener according to the manufacturer recommendations. The physical and mechanical properties of the primer resin and the physical properties of adhesive bonding are summarized in Table (7) and (8) based **[18]**.

Table 7: Physical properties of the Primer resin **[18]**.

Physical properties	
Colour	Translucent
Density	1.12 kg/litre
Thickness of application	100µm
Mechanical properties	
Compressive strength	100 N/mm^2
Tensile strength	19 N/mm^2
Flexural strength	30 N/mm^2
Bond to concrete	> 5.3 N/mm^2
Young's modulus	5 kN/mm^2

Table 8: Physical properties of the bonding adhesive **[18]**

Colour	White, transparent
Density	1.3 kg/litre
Thickness of application	300µm

The surfaces of the concrete blocks, where the CFRP sheet would be glued, were first ground to a fine finish with a stone wheel to remove the top layer of mortar, just until the aggregate was visible (approximately 2-3 mm). Then the concrete surface was properly cleaned with air jet to remove dust. Finally, the surface of the concrete was covered with a thin layer of primer.

Afterwards, the CFRP sheets were applied to both sides of the concrete prisms using two-component epoxy adhesive with a relatively uniform thickness of 1–1.2 mm.

TEST RESULTS AND DISCUSSION

The experimental results of the pull-off double shear-lap tests between the CFRP sheets and the lightweight/normal weight concrete prisms are now presented and discussed in order to understand the bond characteristics, fracture behaviour and the effectiveness of CFRP to retrofit LWC compared to NWC. A summary of the test results are provided in Table 9.

Table 9: Details of LWC and NWC specimens and test results

Test samples	FRP width b_{frp} (mm)	Total CFRP bond length L_{frp} (mm)	CFRP Thickness t_f (mm)	CFRP Orientation	Test failure load P_{test} (kN)	Maximum Slip (s_{max}) (mm)	Test failure Mode
BL1-1a	100	100	0.1178	0^0	19.34	0.30	CF
BL1-1b	100	100	0.1178	0^0	18.71	0.27	CF
BL1-1c	100	100	0.1178	0^0	19.99	0.32	CF
BL1-1d	100	100	0.1178	0^0	19.86	0.37	CF
BL1-2a	100	150	0.1178	0^0	27.31	0.36	CF+DC
BL1-2b	100	150	0.1178	0^0	23.80	0.43	CF+DC
BL1-2c	100	150	0.1178	0^0	27.80	0.50	CF+DC
BL1-2d	100	150	0.1178	0^0	25.22	0.46	CF+DC
BL1-3a	100	200	0.1178	0^0	26.15	0.54	DC+BC
BL1-3b	100	200	0.1178	0^0	27.11	0.56	DC+BC
BL1-3c	100	200	0.1178	0^0	18.50	0.28	DC+BC
BL1-3d	100	200	0.1178	0^0	27.48	0.60	DC+BC
BL2-1a	100	100	0.1178	90^0	0.81	2.3	FR
BL2-1b	100	100	0.1178	90^0	0.57	3.6	FR

BL2-1c	100	100	0.1178	90^0	0.47	0.37	FR
BL2-1d	100	100	0.1178	90^0	0.99	1.4	FR
BL2-2a	100	100	0.1178	45^0	8.24	2.3	DC
BL2-2b	100	100	0.1178	45^0	9.91	2.4	DC
BL2-1c	100	100	0.1178	45^0	9.13	2.5	DC
BL2-1d	100	100	0.1178	45^0	8.76	2.41	DC
BL3-1a	100	100	0.2356	$0^0/0^0$	24.16	0.14	CF
BL3-1b	100	100	0.2356	$0^0/0^0$	22.99	0.16	CF
BL3-1c	100	100	0.2356	$0^0/0^0$	18.19	0.16	CF
BL3-2a	100	100	0.2356	$0^0/90^0$	18.69	0.20	CF
BL3-2b	100	100	0.2356	$0^0/90^0$	19.54	0.23	CF
BL3-2c	100	100	0.2356	$0^0/90^0$	17.72	0.22	CF
BL4-1a	50	150	0.1178	0^0	18.80	0.54	CF+DC
BL4-1b	50	150	0.1178	0^0	13.32	0.58	CF+DC
BL4-1c	50	150	0.1178	0^0	17.31	0.54	CF+DC
BL4-1d	50	150	0.1178	0^0	13.95	0.63	CF+DC
BL4-2a	150	150	0.1178	0^0	21.04	0.043	DC+BC
BL4-2b	150	150	0.1178	0^0	21.69	0.058	DC+BC
BL4-2c	150	150	0.1178	0^0	21.51	0.037	DC+BC
BL4-2d	150	150	0.1178	0^0	20.98	0.039	DC+BC
BN1-1a	100	100	0.1178	0^0	18.13	0.25	DC+AD
BN1-1b	100	100	0.1178	0^0	22.1	0.35	DC+AD
BN1-1c	100	100	0.1178	0^0	21.9	0.32	DC+AD
BN1-2a	100	150	0.1178	0^0	29.6	0.69	DC+AD
BN1-2b	100	150	0.1178	0^0	29.4	0.61	DC+AD
BN1-2c	100	150	0.1178	0^0	28.9	0.63	DC+AD
BN1-3a	100	200	0.1178	0^0	28.4	0.79	DC+AD
BN1-3b	100	200	0.1178	0^0	29.64	0.85	DC+AD
BN1-3c	100	200	0.1178	0^0	28.95	0.67	DC+AD
BN2-1a	100	100	0.1178	90^0	5.13	2.22	FR

BN2-1b	100	100	0.1178	90^0	0.93	2.5	FR
BN2-2a	100	100	0.1178	45^0	10.64	1.61	AD
BN2-2b	100	100	0.1178	45^0	3	0.95	AD
BN3-1a	100	100	0.2356	$0^0/0^0$	28.01	0.18	CF
BN3-1b	100	100	0.2356	$0^0/0^0$	28.19	0.18	CF
BN3-2a	100	100	0.2356	$0^0/90^0$	22.44	0.28	CF
BN3-2b	100	100	0.2356	$0^0/90^0$	23.09	0.28	CF
BN4-1a	50	150	0.1178	0^0	14.80	0.53	CF+AD
BN4-1b	50	150	0.1178	0^0	15.55	0.57	CF+AD
BN4-2a	150	150	0.1178	0^0	29.05	0.153	DC+BC
BN4-2b	150	150	0.1178	0^0	29.69	0.17	DC+BC

Note: (a) CF, Concrete prism failure (b) DC, debonding in concrete (c) BC, bond failure between the steel bar and the concrete, (d) FR, CFRP rupture (e) AD, Adhesive debonding, (f) t_f is the one side thickness of CFRP sheet.

Failure condition

In general, the failure conditions of the LWC samples were due to crack propagation within the concrete. This led to a brittle failure of the concrete and sometimes resulted in concrete debonding. In contrast, the most common failure observed in the NWC samples was concrete debonding and sometimes adhesive debonding. The crack intensity was more prevalent in LWC specimens compared to NWC specimens. Figure 3(a) and (b) compares the concrete failure between LWC and NWC respectively. The higher peeling width and thickness in the LWC samples compared to similar strength NWC may be due to the lower shear strength for Lytag aggregates compared to that of normal aggregates.

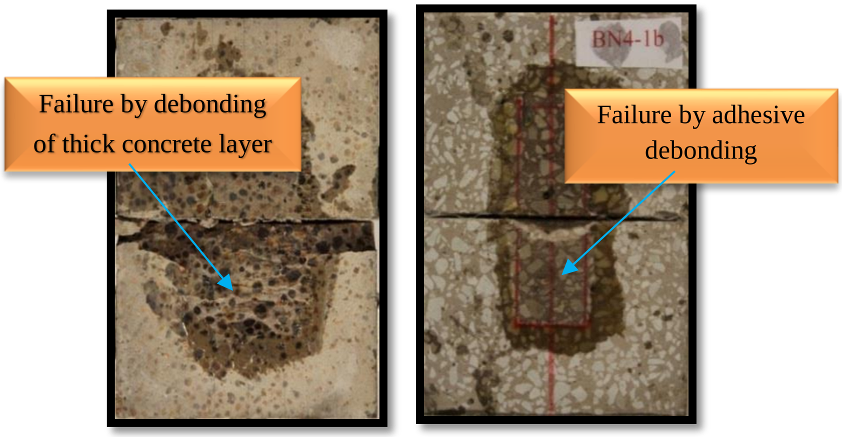

(a) LWC samples (b) NWC samples

Figure 3: Comparison of failure modes between LWC and NWC samples

As bond failure developed in the BL1-1, BL3-1, BL3-2 and BL4-1 specimens, small diagonal cracks started to occur at the centre of the specimen. These cracks never extended significantly outwards from the centre of the samples. The angle of the cracks suggests an edge effect, affecting the crack front propagation. This is the same failure observed by **[19&20]** prior to our study. As more load was applied, these samples developed additional small cracks near the center of the concrete prism. Once the cracks appeared, they propagated rapidly towards the upper surface of the tested concrete sample, which led to sudden brittle failure of the concrete prism by the formation of a diagonal fracture plane as shown in Figure 4 (a) and (b). The same failure mode was observed for the NWC samples of the (BN3-1) and (BN3-2) series as shown in Figure 4 (c) and (d).

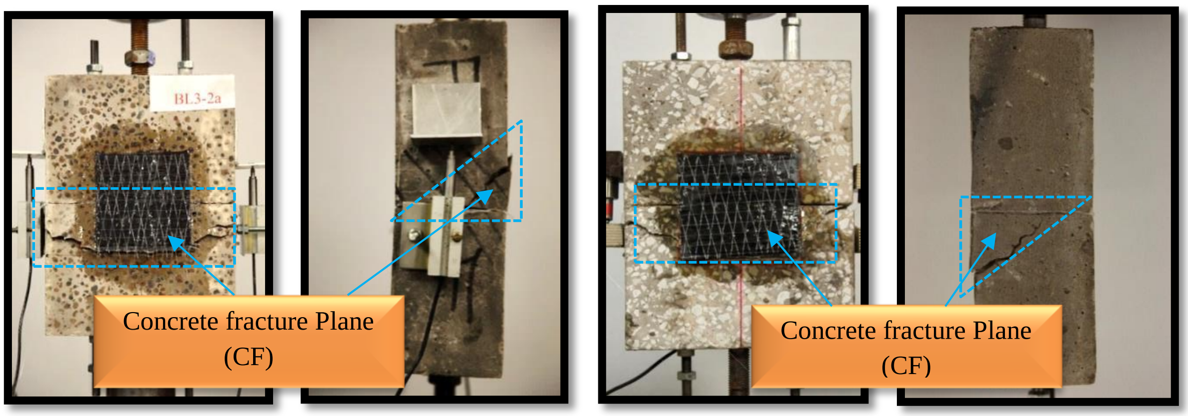

(a) (b) (c) (d)

Figure 4: Typical failure in the concrete prism (CF) in LWC and NWC specimens (a) Front view of LWC specimen, (b) Side view of LWC specimen, (c) Front view of NWC specimen, (d) Side view of NWC specimen.

All the samples of BL1-2, BL1-3 and BL4-2 and BN4-2 series failed due to concrete debonding adjacent to the adhesive-concrete interface, where concrete layers of different thickness were broken and attached to the CFRP sheet. The debonding failure between the CFRP sheet and the concrete was extremely brittle and the duration of the debonding process was mainly influenced by the bond area. The failure process started with small concrete cracking near the specimen center. As the load increased, the small cracking in the concrete initiated CFRP debonding from the concrete surface near the sample centre and then propagated towards the far end of the FRP sheet. This eventually led to full detachment of CFRP strips from the concrete surface as shown in Figure 5 (a) and (b). Splitting cracks along the plane of the loaded steel bar developed in some of the (BL1-3) and (BL/N4-2) samples at very high loads leading to sudden bond failure between the steel bar and the concrete followed by concrete debonding.

The samples of the BN1-1, BN1-2, BN1-3 and BN4-1 series showed a combined failure mode as shown in Figure 5(c) and (d). All these samples failed by debonding of small pieces of concrete near the sample centre followed by adhesive debonding. This may be attributed to the higher stiffness of normal weight particles and the surrounding cementitious matrix. The matrix resists the crack propagation from the centre of the concrete sample toward the far end, which leads to stress concentration. The result is debonding of the concrete near the centre of the sample.

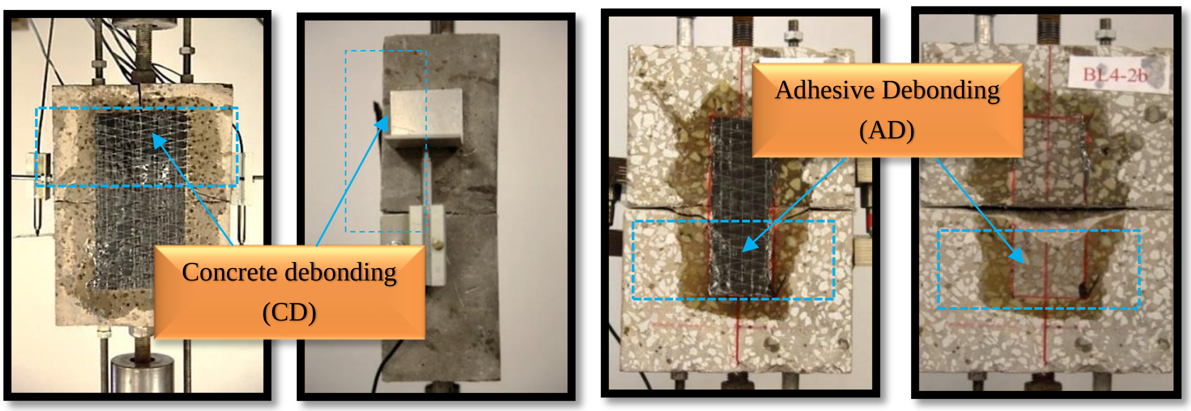

(a) (b) (c) (d)

Figure 5: Typical combined failure concrete debonding of LWC and NWC specimens: (a) front view of LWC specimen, (b) side view of LWC specimen, (c) front view of NWC specimen, (d) front view of NWC specimen without CFRP sheet.

CFRP strain and local shear stress distribution

Data is collected from strain gauges mounted on the upper surface of the CFRP sheet on one side of the three specimens in each BL1-1, BL1-2 and BL1-3 series and two specimens of each BN1-1, BN1-2 and BN1-3 series. These data are used as an example to understand the process of debonding and to show the typical strain distribution profile along the length of the CFRP sheet. Figure 6 shows the distributions of strain at different levels of maximum load (40%, 60%, 80%, 90% and 100% of the maximum load) for LWC and NWC samples with different bonded lengths. Each curve plotted corresponds to the strain distribution along the CFRP sheets at a particular load. When the load (P) is smaller than about 60% of the maximum load (P_{max}), the

CFRP strain decreases quickly with distance from the center of the concrete prism. This descending trend is attributed to the low axial stiffness of the bonded CFRP composite sheet with respect to that of the concrete sample. Increasing the load before primary debonding leads to upward shifting of the curve, but the strain trend does not change. However, when the load value goes beyond 60% of maximum load, cracks start to develop. The cracking led to a clear change of the strain distribution in the CFRP sheet. The profiles tended to attain a linear shape and the slope of the strain curve tended to decrease near the specimen center. Since the slope of the curve reflects the rate of strain change in the CFRP Sheet (which is proportional to the local shear stress), the decrease of the slope shows shear softening along the FRP-concrete interface. The same behaviour was observed in a previous study **[20&21].** At a certain load level before local debonding, the strain profile at the beginning of the bonded length almost remains constant up to the failure of the joint. This means that the concrete prism begins failure at the loaded end. It also follows that the portion of the CFRP sheet near the loaded end of the specimen cannot transfer load. The strain gauges far from the center measure strain which indicates the load transfer zone shifted away from the loaded end of the specimens towards the centre of the sample.

In this paper, the "Active zone" is defined as the distance between the point of the maximum strain at the centre of the sample and the point of the minimum strain. The strain distributions of the NWC samples with 50 mm bonded length have been plotted in Figure (6a). The patterns of strain distribution of these samples were similar to those obtained for LWC samples as shown in Figure (6d). The active zone length was approximately 50 mm up to the maximum load level. The maximum recorded strain reading for the LWC samples was approximately 4600 µm/m and 3600 µm/m for the NWC samples. Figure (6b) shows the strain distribution of the NWC samples with 75 mm bonded length. It can be noted that the active zone moved to 75mm at the maximum load level. The same behaviour was observed for samples cast with LWC with 75 mm bonded length as explained in Figure (6e). The maximum recorded strain reading was approximately 6800 µm/m for the LWC and NWC samples. Figure (6c) shows the strain distribution of the NWC samples with 100 mm bonded length. No more movement was observed for theses samples. The active transfer zone ranges between 70-75 mm. Similar behaviour was observed for samples cast with LWC with 75 mm bonded length as shown in Figure (6f). The maximum recorded strain reading was approximately 8300 µm/m for LWC specimens and 4800 µm/m for NWC samples. It can be concluded that both LWC and NWC samples showed the same strain distribution patterns along the length of the CFRP composite. However, the LWC specimens recorded higher strain readings compared to NWC in most cases. This is strongly related to higher crack intensity due to the lower shear strength of Lytag aggregates, which allows propagation of the cracks over a large area of the concrete substrate. This contrasts with that of natural weight aggregates. The noticeable difference between the LWC samples and NWC in terms of strain distribution is as follows: for LWC, the strain gauges attached near the far end of the CFRP sheet detect more strain compared with samples cast with NWC. This is attributed to local concrete debonding near the far end of the CFRP sheet.

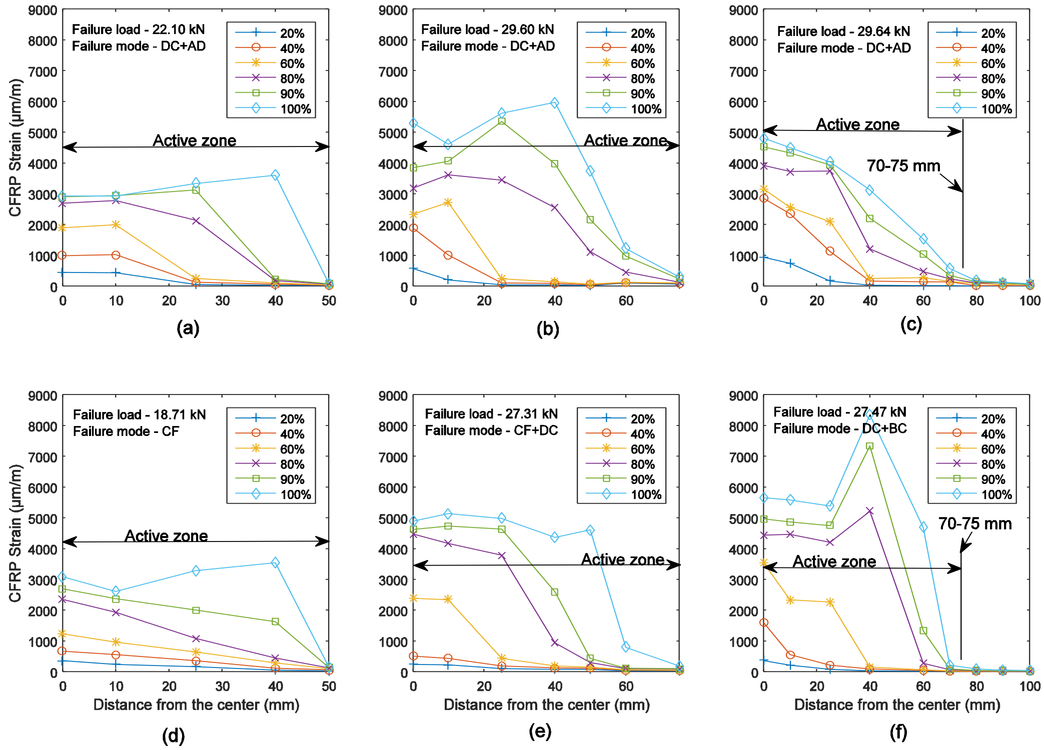

Figure 6: CFRP strain versus distance from the centre of the specimens (a) BN1-1, (b) BN1-2, (c) BN1-3, (d) BL1-1, (e) BL1-2 and (f) BL1-3

Effect of concrete type on interfacial bond strength

LWC bond test specimens showed 73%-96% lower bond strength and slightly lower slip at failure than those of NWC of similar strength grade, regardless of the CFRP strengthening system. Considering the average bond strength of each series, a linear regression analysis was carried out on the results between the NWC and LWC samples. Linear regression analysis shows that the bond strength of LWC is approximately 0.85 of the NWC samples having the same strengthening techniques as shown in Figure 7.

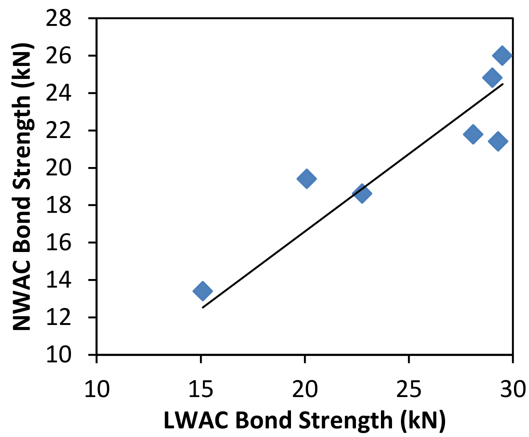

Figure 7: Relationship between the bond strength of LWC and NWC samples

Debonding of the samples in lap shear tests mainly occurs inside the concrete. Furthermore, interlocking along the debonding plane may affect the bond behaviour in samples cast with LWC. The bond capacity is dependent on the residual friction along the attached area of the CFRP. Therefore, the composition of the concrete needs to be considered in the study of interfacial behaviour in adhesively bonded joints. The effect of LWC should be considered in the current design guidelines by introducing a safety reduction factor due to the lower surface tensile strength. The lower strength accelerates substrate failure compared with NWC samples which show higher debonding loads.

The fundamental difference between normal and lightweight aggregate concrete is the tensile strength, which influences the aggregate interlock. The shear capacity of the RC members is proportional with the aggregate interlocking effect **[22]**. In lightweight concrete retrofitted with epoxy bonded FRP for shear deficiencies, the failure path is in the substrate of concrete due to lower aggregate interlock. The efficiency of using FRP is not fully exploited in lightweight concrete. In contrast, the failure was due to debonding of FRP along the bonding agent. This effect of the aggregate interlocking on the maximum shear capacity is hard to control in experimental tests because it depends on the type, size and the distribution of these aggregates in the debonding plane. Lower stiffnesses of lightweight aggregate particles and higher cement ratio result in large plastic deformation. In addition to higher crack intensity in LWC compared with those samples cast with NWC are likely to increase the shear and normal stresses in FRP reinforcements and at the concrete-FRP interface. An increase in interfacial and normal stresses may be lead to FRP debonding, thus the effectiveness of FRP for shear strengthening (LWC) elements is slightly affected by these issues.

Effect of CFRP sheet length

The three cases of the BL/N1-1, BL/N1-2, and BL/N1-3 series have the same width and thickness (w_f=100 mm and t_f=0.1178 mm) and have different bonded length of the CFRP sheet (50, 75, and 100 mm). The bonded length measured from the center of the specimens to the far end of the CFRP sheet in one side of the concrete sample is clarified in Figure (2d). Test results indicate that the increase of CFRP sheet length beyond 75 mm does not lead to higher load capacity in both LWC and NWC samples. However, a larger bond length leads to a longer deformation process as debonding propagates along the interface. Based on the failure mechanism, the effective bond length was assumed to be about 75 mm for LWC and NWC samples, which showed the same behaviour. It can be concluded that the effective bond length is not influenced by concrete type. Figure 8 presents the effect of increasing the bond length of the CFRP sheet on the maximum load. The load-slip relationship for one sample has been selected from each testing series with various CFRP bond lengths, as these are all similar in shape. The load increases linearly with increase in slip and after a certain stage shows nonlinear behaviour. The post-nonlinear stage for the samples shows the same trend in each series. There is no significant difference in behaviour for specimens with different bonded lengths. However, increasing the CFRP bonded length leads to concrete debonding in addition to concrete failure which was observed in this test. It can be seen that the load-slip curve appears to be a plateau for LWC and NWC samples with 75 mm and 100 mm bonded length where the load continues to increase and drop repeatedly within a narrow range of load values, until complete debonding of the CFRP sheet from the concrete substrate. This supports the concept of an effective length of the CFRP sheet. For further comparison, Figure 9 shows the changes in the normalized load ratio (P_a / $P_{a,\ max}$). The $P_{a,max}$ value used in this study for comparison is the average of maximum load for (BL1-2) and (BN1-2) specimen's series from both LWC and NWC, while P_a value is the average of maximum achievable load for specimens with 50 mm, 75 mm and 100 mm bonded length. When the bonded length changed from 50 mm to 75 mm in LWC samples, the normalized load ratio increased by about 34%; beyond 75 mm bonded length. The maximum load did not increase significantly and in fact decreased by about 5%. For NWC samples, the changing of the bonded length from 50 mm to 75 mm leads to increase the normalized load ratio by 47 %. Beyond 75 mm bonded length, the maximum debonding load did not increase significantly and in fact decreased by about 1.6%. The effective bond length is determined based on "Active zone length", and is defined as the distance between the points corresponding to maximum strain at the centre of the sample and the point of zero strain near the far end of the CFRP sheet. The maximum active strain zone ranges between 70-75 mm. Therefore, the bonded length of the CFRP sheets in the LWC and NWC series of tests is considered to be at least 75mm in length. It can also be observed that there is no significant difference in behaviour for specimens with different bonded lengths. However, the increased CFRP bonded length leads to concrete debonding in addition to concrete failure for LWC samples or concrete debonding followed by adhesive debonding in the case of NWC samples which were observed in this test.

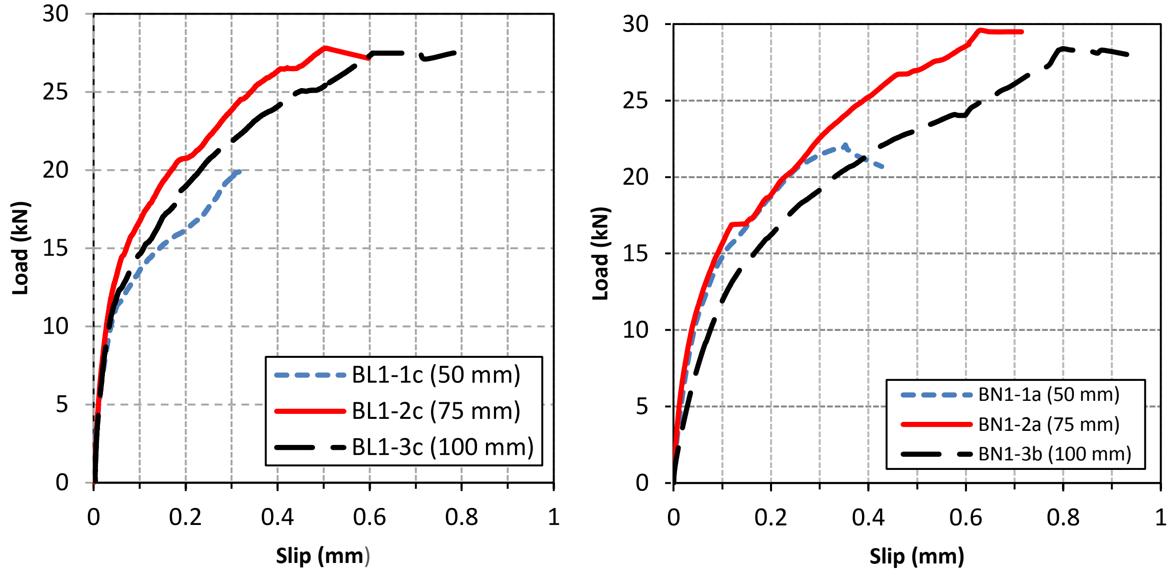

(a) LWC samples (b) NWC samples

Figure 8: Influence of CFRP bond length on the maximum load of the tested samples.

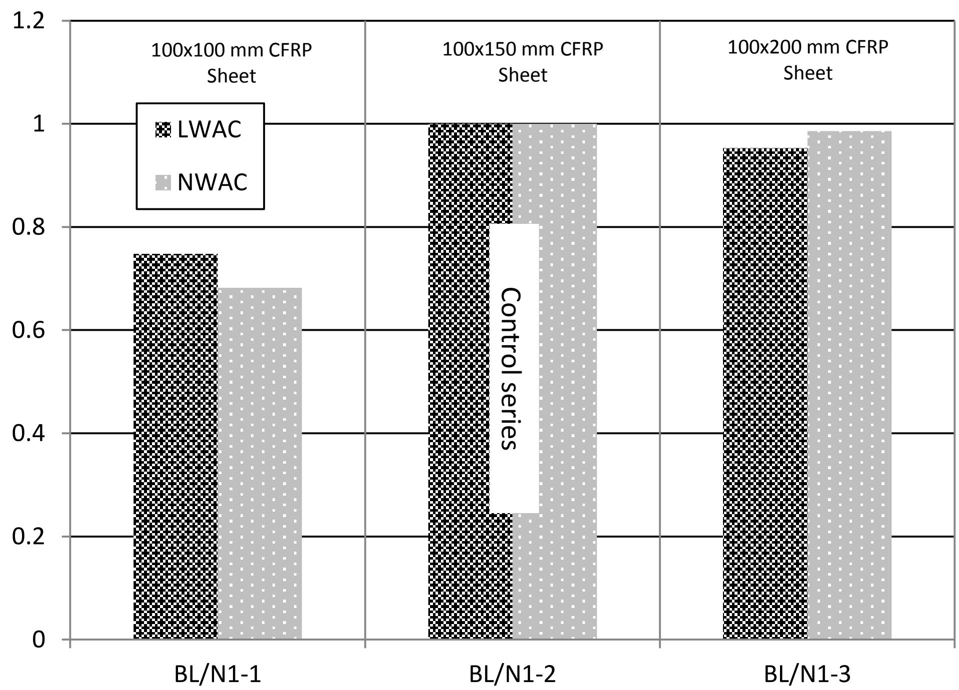

Figure 9: Normalized Load ratio comparison for CFRP bonded length

Effect of orientation of the CFRP sheet on bond behaviour

The fibre orientation of the CFRP sheet is one of the parameters that most influences the interfacial behaviour between the concrete and FRP composite. All the specimens were subjected to pure tensile force. Therefore, if there is an angle between the load and fibre direction, this tends toward a lesser contribution of the CFRP sheet to the sample strength. It is seen that the specimens of BL/N2-1 series did not fail at any significant load. Failure of BL/N2-1 specimens was abrupt at a small load because the two concrete parts separated at the center of the specimens without any resistance. By examining Figure 10, the initial stiffness for the load-slip plot decreases as the fibre angle increases with respect to load direction. The noticeable thing in this figure is that the LWC samples strengthened with 45^0 fibres orientation of the CFRP sheet initiates more cracks near the specimen's center, which propagated in a stable manner through the CFRP- concrete interface until failure occurred. This crack propagation is accompanied by a drop in rigidity easily highlighted by the nonlinearity of the load-displacement plots for these samples. Figure 11 shows the variation of the normalized maximum load ratio versus the fibres' orientation of CFRP composite for both LWC and NWC mixture. It can be concluded that the increasing of the fibres' angle with respect to load direction from 0^0 to 45^0 decreases the normalized load ratio by 51% compared with the companion samples BL1-1 for specimens cast with LWC and 66% for NWC specimens. With further increasing of the angle to [90^0], the load ratio decreases by 97 % for LWC samples and 89% for NWC samples. This is attributed to the nature of the CFRP composite properties, which is classified as an orthotropic material having different properties in different directions with the maximum strength being parallel to the fibre direction.

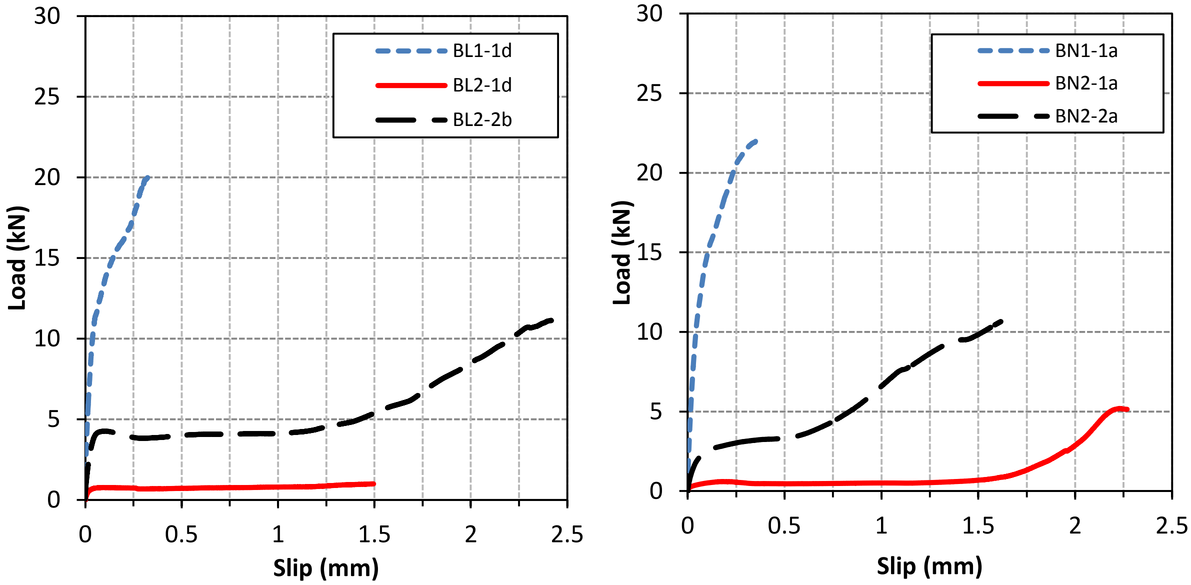

(a) LWC samples (b) NWC samples

Figure 10: Influence of CFRP fibre orientation of tested samples

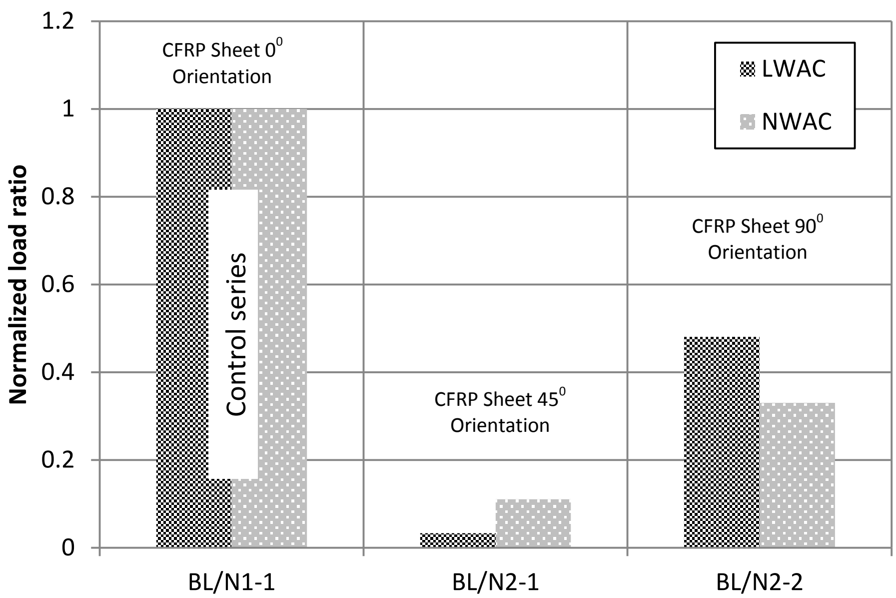

Figure 11: Effect of the fibre orientation on the normalized load ratio.

Effect of CFRP sheet thickness on bond

The experimental results of the three cases of the BL/N1-1, BL/N3-1, and BL/N3-2 series with the same dimensions and different bonded thickness and orientation of CFRP sheet are used to examine the influence of using two parallel and perpendicular layers of CFRP composite. It can be noticed that the failure of all the specimens are categorized as concrete failure (CF). For LWC samples, the increase in the normalized load ratio from one to two parallel layers [$0^0/0^0$] was approximately 12%, while the change of strengthening technique from one to two perpendicular layers [$0^0/90^0$] does not provide any contribution as shown in Figure 12. This means that increasing the thickness of the CFRP sheet provides limited benefit for strengthening. In contrast, the difference between the normalized load ratios of BN3-1 (same direction) and BN1-1 is approximately 39%. Besides this, the difference in average load ratio of BN3-2 (two perpendicular layers) of the CFRP sheet compared with BN1-1 is about 12% as shown in Figure 12. It can be concluded that the load capacity for double parallel layered specimens is higher than the load of double perpendicular layered specimens. This means that if the load direction is parallel to two layers, this scenario is better than having double perpendicular layers regardless of orientation to the load. For more investigation, Figure 13 shows the comparison of load-slip response for the three cases. As shown in these figures, the initial stiffness of the CFRP-concrete joints with the [$0^0/0^0$] sheet is higher than that of the [$0^0/90^0$] sheet and for samples with one layer [0] sheet. This high stiffness appears to promote a higher failure load and lower slip compared with other cases. A similar response was observed for both LWC and NWC samples. Therefore, it can be concluded that when the strength criteria governs the design for the strengthening of reinforced concrete structures, an increase in the CFRP stiffness may lead to higher load carrying capacity. However in the case of ductility, higher stiffnesses lead to extremely brittle adhesively bonded joints, particularly for LWC, which shows a propensity for brittle behaviour compared with NWC specimens.

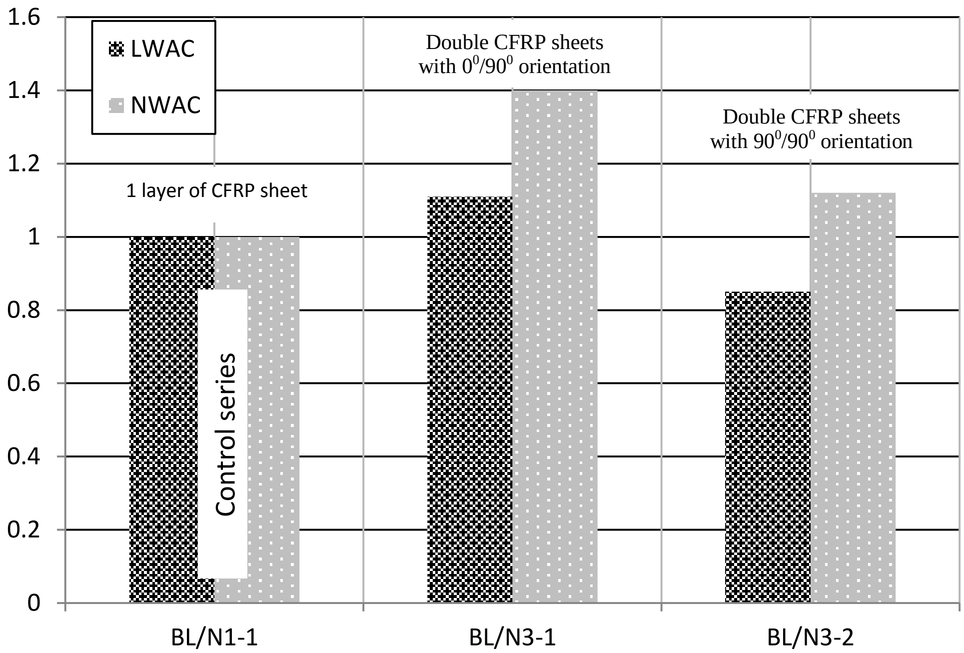

Figure 12: Effect of CFRP sheet thickness on the normalized load ratio.

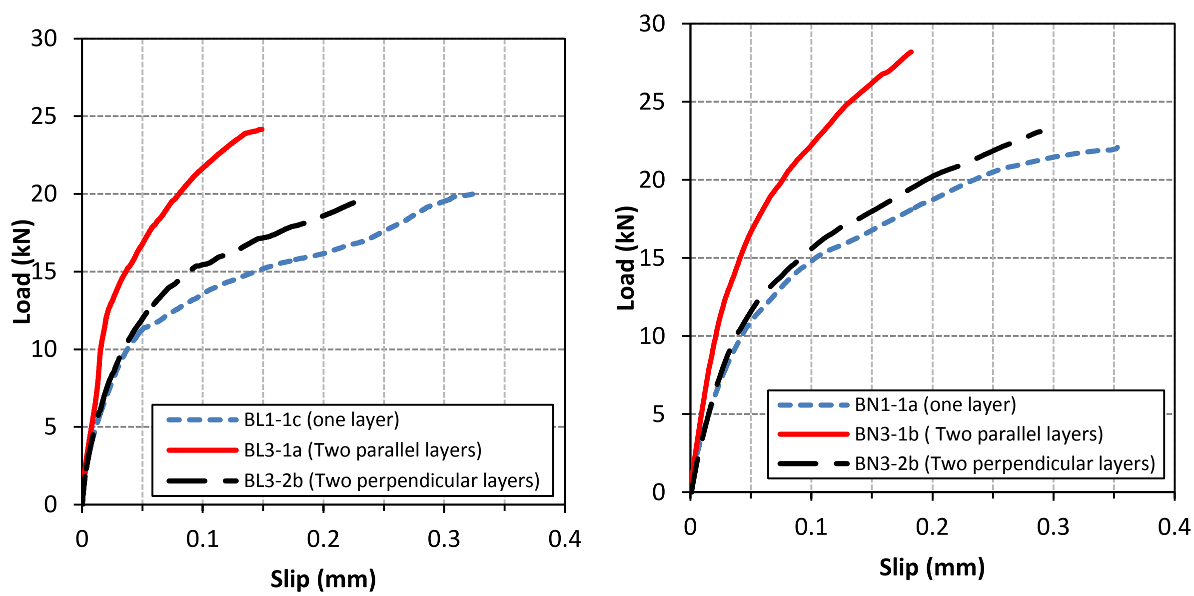

(a) LWC samples

(b) NWC samples

Figure 13: Influence of CFRP bond thickness of LWC and NLW samples

Effect of CFRP-to-concrete width ratio on bond behaviour

The effect of FRP to concrete width ratio ($w_r = b_f/b_c$) on the interface behaviour is examined in the samples BL/N4-1, BL/N1-2, and BL/N4-2 (see Figure 14). All these samples have the same thickness (t=0.1178 mm), bonded length of CFRP composite (L_{frp}=75 mm) and various width of CFRP sheet (50, 100, and 150 mm).The CFRP-to-concrete width ratios are 0.25, 0.5 and 0.75 respectively. It may be noted that with increase in width, the maximum load increases when the width ratio is changed from 0.25 to 0.5 for both LWC and NWC samples. This trend may be attributed to the distribution of shear stresses over a larger bonded area. However, increasing the width ratio to 0.75 leads to premature sample failure at load lower than the failure of samples with 0.5 width ratio in the case of LWC samples or approximately the same load for samples with 0.5 width ratio in case of NWC samples, as shown in Figure 14. In this case, the width of concrete samples is not sufficient to allow the propagation of the stress from the CFRP into the substrate. Therefore, the level of confinement to the CFRP decreases, which accelerates the failure of the interfacial bonded joint at lower loads. Nevertheless, the average bond strength may not increase using wider CFRP reinforcement. The bond behaviour described above was also observed in previous work [**23&24]**. It can be concluded that increasing the CFRP sheet widths leads to concrete debonding accompanied by bond failure between the concrete and steel bars for both LWC and NWC samples. The slip corresponding to the width ratio at the maximum load decreases by a higher value of CFRP-to-concrete width ratio. This indicates that ductility of the CFRP–concrete interface decreases for a wider CFRP sheet.

Considering Figure 15, the specimens show higher initial stiffness for the load-slip plot, when the FRP width increases versus the concrete prism width. Micro-cracks have sufficient space to propagate across the wider bonded area of the CFRP composite. When the macro-crack initiates, the possibility to cross micro-cracks on its way is greater. These micro-cracks help to bind the macro-crack during the loading process. Therefore, the bond between the wider CFRP sheet and the concrete surface is stronger in comparison with those samples that have lower CFRP-to-concrete width ratio.

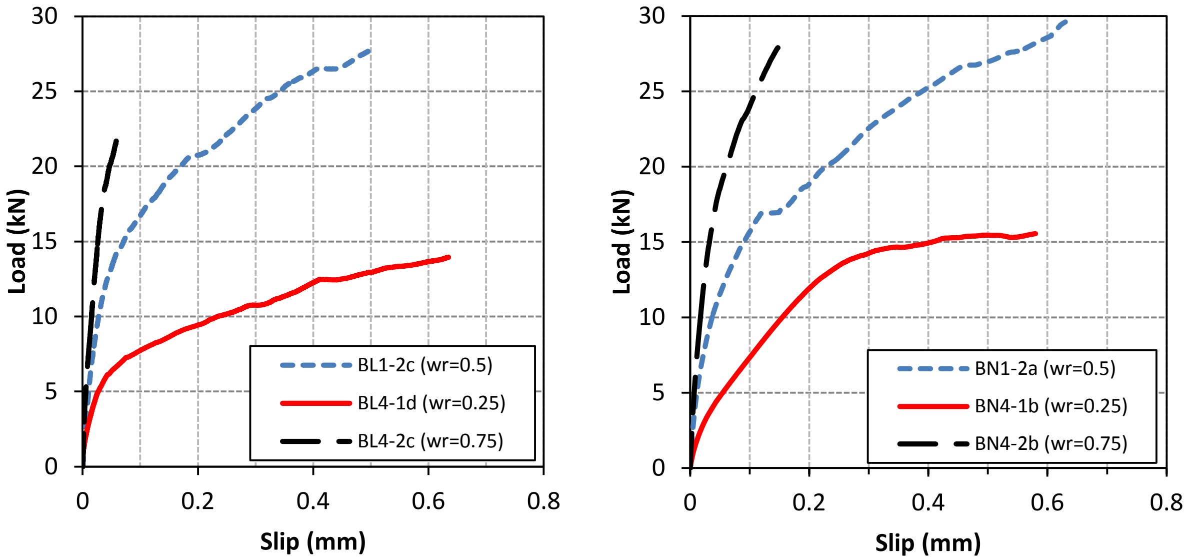

(a) LWC samples (b) LWC samples

Figure 14: Influence of CFRP width on the tested samples.

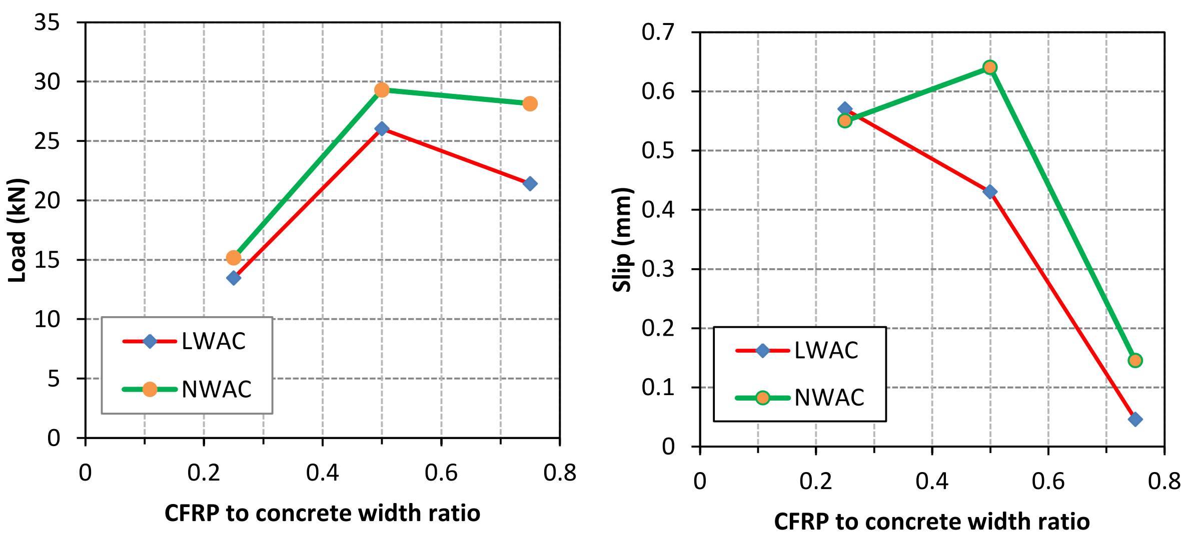

(a) (b)

Figure 15: Correlation between FRP-to-concrete width ratio and (a) the maximum load (b) slip.

COMPARISON WITH EXISTING THEORETICAL MODELS

Most existing numerical models for prediction of bond strength and effective bond length were developed using normal weight concrete. The current experimental results show that the modes of failure for LWC and NWC are different. Furthermore, the LWCs' failure loads were slightly less than those of NWC. In order to assess the use of existing models in LWC, the models and guidelines proposed by FIB 14 **[25]**, TR-55 **[26]** , Seracino et al. **[27]** and Serbescu et al. **[28]** are considered in this study.

The maximum bond between concrete and FRP composite, P_{max} and the effective bond length, L_e according to FIB 14 **[25]** is as follows:

$$P_{max} = \alpha . c_1 . k_c . k_b . b_f . \sqrt{E_f . t_f . f_{ctm}} \tag{1}$$

$$k_b = 1.06 . \sqrt{\frac{2 - b_f/b_c}{1 + b_f/400}} \geq 1.0 \tag{2}$$

$$L_e = 0.7 \sqrt{\frac{E_f . t_f}{c_2 . f_{ctm}}} \tag{3}$$

$$P_{\max} (L_f < L_e) = \left(P_{max} . \frac{L_f}{L_e}\right)\left(2 - \frac{L_f}{L_e}\right) \tag{4}$$

where P_{max} , L_f and L_e are the maximum debonding load, FRP bond length, and effective bond length respectively; b_f, t_f, and E_f are the width, thickness and Young's elasticity modulus of the FRP reinforcement respectively; b_c is the width of the concrete element; $f_{ctm}$is the mean tensile strength of concrete, α is a reduction factor, approximately equal to 0.9, to account for the influence of inclined cracks on the bond strength; k_c is a factor accounting for the state of compaction of concrete (generally it can be assumed to be equal to 1.0); k_b is a geometry factor presented by Equation (2). Note that c_1 and c_2 in Equations (1) and (3) may be obtained through calibration with test results. However, for CFRP strips, c_1 and $c_2$are equal to 0.64 and 2.0 respectively. Moreover, for bond lengths, $L_f < L_e$ the ultimate debonding load can be calculated by Equation (4).

The maximum debonding load of FRP reinforcement, P_{max} and the effective bond length, $L_e$in TR-55 **[26]** are assessed based on the following expressions.

$$P_{max} = 0.5 \,.\, k_b \;\; b_f \,.\, \sqrt{E_f . t_f . f_{ctk}} \tag{5}$$

$$L_e = 0.7 \sqrt{\frac{E_f . t_f}{f_{ctk}}} \tag{6}$$

$$P_{\mathrm{max}}\ (L_f < L_e) = \left(P_{max} . \frac{L_f}{L_e}\right)\left(2 - \frac{L_f}{L_e}\right) \tag{7}$$

where P_{max}, L_f and L_e are debonding load, FRP bond length, and effective bond length respectively; b_f, t_f, and E_f are the width, thickness and Young's elasticity modulus of the FRP reinforcement respectively; b_c is the width of the concrete element; f_{ctk} is the characteristic tensile strength of concrete and f_{ctm} is the mean tensile strength of concrete. Similar to FIB 14, k_b can be calculated using Equation (2).

The maximum debonding load and effective length of FRP reinforcement based on Seracino et al. **[27]** model can be obtained from the following expressions:

$$P_{max} = 0.85 \left(\frac{d_f}{b_f}\right)^{0.25} . (f_c')^{0.33} \;\; . \sqrt{L_{per} E_f t_f} \tag{8}$$

$$L_e = \frac{\pi}{2\sqrt{\tau_f . L_{per} / \delta_f . E_f . A_f}} \tag{9}$$

$$\tau_f = \left(0.802 + 0.078 \frac{d_f}{b_f}\right) (f_c')^{0.6} \tag{10}$$

$$\delta_f = \frac{0.73}{\tau_f}\left(\frac{d_f}{b_f}\right)^{0.5} (f_c')^{0.67} \tag{11}$$

$$P_{\max}\ (L_f < L_e) = \left(P_{max}.\frac{L_f}{L_e}\right) \tag{12}$$

where A_f is the transversal area of FRP composite; d_f is the thickness of the failure plane perpendicular to the concrete surface, which is proposed as 1mm; L_{per} is the length of the debonding failure plane, which can be obtained as $2d_f + b_f$. Moreover, τ_f and δ_f are the peak local shear stress and slip respectively, beyond which bond stress is zero..

The maximum debonding load of the FRP composite, P_{max}, and the effective bond length, L_e, based on Serbescu et al. **[28]** are evaluated based on the following expressions:

$$P_{max} = \frac{2}{3}\ .\beta\ .\frac{455}{b_f + 350}\ \left(0.8.\sqrt{f_{cu}}\right)\ L_e\ .b_f \tag{13}$$

$$L_e = 0.7\sqrt{\frac{E_f.t_f}{2.8\,f_{ctm}}} \tag{14}$$

where β is the surface preparation coefficient, which is assumed to be 0.85 (recommended preparation). Moreover, f_{cu} and f_{ctm} are the mean cube compressive strength and mean tensile strength of concrete.

The coefficient of variation of the predicted bond strength for the LWC and NWC are summarised in Figure 16 (a) and (b). A certain disparity is apparent between the NWC and LWC results. The NWC results show closer agreement than those of the LWC results. It can be seen that the model suggested by Seracino et al. **[27]** resulted in the highest coefficients of variation among the predicted to-experimental debonding failure loads for specimens cast with LWC and NWC. This model is slightly conservative and calibration cannot easily be applied, since the model proposed is based on d_f (thickness of the failure plane) and such a variable is not easy to obtain based on limited experimental tests.

On the other hand, the model proposed by FIB 14 **[25]**, TR-55 **[26]** and Serbescu et al. **[28]** show that the lowest values of the coefficient of variation (CV) were a result of the fact that they consider the effect of the width of the FRP sheet and the concrete tensile strength in calculating the maximum debonding loads. The average predicted to experimental bond strength of the LWC and NWC specimens are summarised in Table 10.

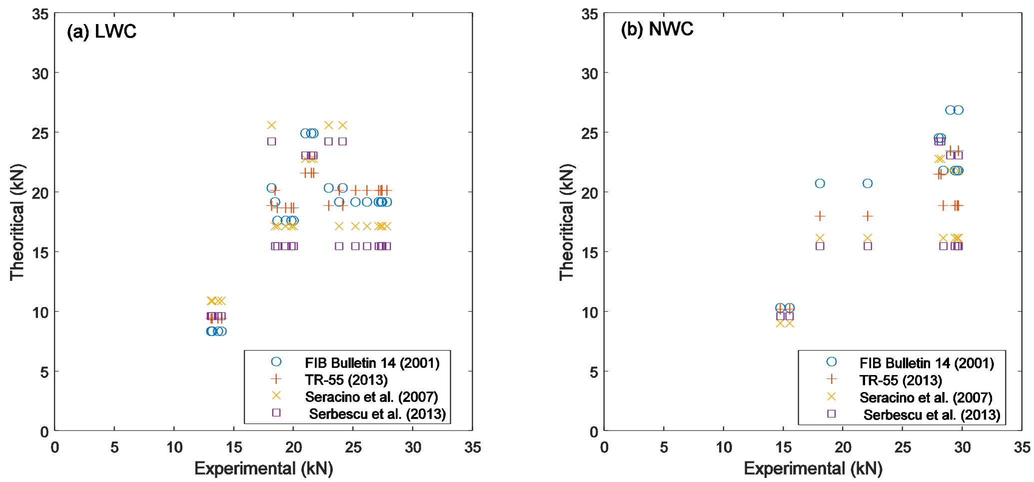

Figure 16: Theoretical prediction load vs experimental observation of (a) LWC and (b) NWC

Table 10: Average predicted to experimental bond strength of the LWC and NWC specimens

	Theoretical to experimental loads($P_{theoretical}$ / $P_{experimental}$)							
	TR-55 (2013)		FIBFIB Bulletin14		Seracino et al.		Serbescu et al.	
	LWC	NWC	LWC	NWC	LWC	NWC	LWC	NWC
AVG	0.85	0.73	0.84	0.83	0.79	0.68	0.86	0.67
STDEV	0.13	0.10	0.18	0.13	0.21	0.14	0.2	0.12
COV (%)	15.29	13.6	21.4	15.6	26.5	20.5	23.2	17.9

The theoretical effective bond lengths of the CFRP sheet for both LWC and NWC tested samples predicted by FIB 14**[25]**, TR-55 **[26]** guidelines and models developed by Seracino et al. **[26]** and Serbescu et al. **[28]** are used in this study to evaluate the experimental effective length. The calculated L_e based on the FIB 14**[25]**, TR-55 **[26]** guidelines and Serbescu et al. **[28]** are about 69.8 mm, 69.1 mm and 59 mm respectively for LWC samples, while the predicted effective length for NWC samples is about 64.4, 63.8 mm and 54 mm respectively. Note that slight differences in predicted L_e for tested specimens between LWC and NWC are due to the variation of tensile strengths of different concrete types. The predicted effective length based on Seracino et al. **[27]** is about 33 mm for both LWC and NWC.

The experimental results show that increasing the bond length (L) beyond 75 mm has no significant effect on maximum debonding capacity, and maximum loads are approximately constant when L increases beyond 75 mm. Consequently, as mentioned in this paper the experimentally evaluated effective length for the CFRP sheets of the current study is approximately equal to 75 mm. Comparing the experimentally evaluated effective length with the theoretically calculated values show that the model of Seracino et al**. [27]** underestimates the effective length of the CFRP sheet, while the other model and guidelines provide more realistic values for the effective length in most cases.

CONCLUSIONS

The interfacial behaviour of LWC was studied in this research. For this purpose, 55 concrete blocks (34 LWC prisms and 21 NWC prisms) were cast and tested using the modified double lap shear test set-up. The bonded length, width and direction of uni-directional bonded CFRP sheets were varied in order to understand the fracture behaviour and the effectiveness of CFRP. Overall, the experimental results show that the crack propagation occurred within the LWC specimens, while peeling of CFRP was the main cause of failure mechanism in NWC specimens. The effectiveness of using FRP to retrofit RC structures is mainly affected by the concrete properties. Since the existing design codes and numerical models were developed based on test data of normal weight concrete, the performance of FRP with LWC was investigated. From the experimental tests, a number of conclusions can be derived.

1. In general, LWC bond test specimens showed significantly lower bond strength and slightly lower slip at failure than those of NWC of similar strength grade.
2. The results of this study showed that the increase of CFRP sheet length beyond 75 mm does not lead to higher load capacity in both samples cast with LWC and NWC. However, a larger bond length leads to a longer deformation process as debonding propagates along the interface. The effective bond length was assumed to be about 75 mm for LWC and NWC samples, which showed the same behaviour. It can be concluded that the effective bond length is not influenced by concrete type.

3. The orientation of the CFRP sheet is one of the parameter that most influences the behaviour which is critical in shear retrofitting system. Therefore, if there is an angle between the load and the fibre direction, this tends toward a lesser contribution of the CFRP sheet to the strength. No significant difference in behaviour was observed between LWC and NWC samples and the same failure modes were recorded for samples having different fibre orientation.
4. The CFRP sheet thickness has the same influence on the interfacial behaviour of the LWAC and NWC samples. However, LWAC recorded lower debonding load compared with NWC samples.
5. If there is an increase in the CFRP-to-concrete width ratio, the maximum load carrying capacity is increased. This may be attributed to the distribution of shear stresses over a larger area of the bond. However, for large values of CFRP-to-concrete width ratio, load carrying capacity decreases with wider CFRP. In the latter case, the width of concrete samples is not enough to allow the propagation of the stress from the CFRP into the substrate. Therefore, the level of confinement to the CFRP decreases, which accelerates the failure of the interfacial bonded joint in lower loads.

REFRENCES

1. Rousan R., Issa M., **Fatigue performance of reinforced concrete beams strengthened with CFRP sheets**. Journal of Construction and Building Materials **25**, 3520–3529 (2011).
2. Cottone A., Giambanco G., **Minimum bond length and size effects in FRP–substrate bonded joints**, Journal of Engineering Fracture Mechanics **76**, 1957–1976 (2009).

3. Pellegrino C., Tinazzi D., and Modena C., **Experimental Study on Bond Behaviour between Concrete and FRP Reinforcement**. Journal of Composites for Construction, **12 (2)**, 180-189 (2008).
4. Chajes, M. J., Finch Jr, W. W., Januszka, T. F. and Thomson Jr, T. A. (1996). **Bond and force transfer of composite material plates bonded to concrete**. ACI Structural Journal, 93(2), 208-17.
5. De Lorenzis, L., Miller, B. and Nanni, A. (2001). **Bond of FRP laminates to concrete**. ACI Materials Journal, 98(3), 256-64.
6. López-González, J., Fernández-Gómez, J. and González-Valle, E. (2012). **Effect of Adhesive Thickness and Concrete Strength on FRP-Concrete Bonds**. Journal of Composites for Construction, 16(6), 705-11.
7. Nakaba, K., Kanakubo, T., Furuta, T., & Yoshizawa, H. (2001). **Bond behaviour between fiber-reinforced polymer laminates and concrete**. ACI Structural Journal, 98(3), 359-367.
8. Woo, S. K. and Lee, Y. (2010). **Experimental Study on Interfacial Behaviour of CFRP Bonded Concrete. KSCE Journal of Civil Engineering**. 14(3), 385-93.
9. Subramaniam, K. V., Carloni, C. and Nobile, L. (2007). **Width effect in the interface fracture during shear debonding of FRP sheets from concrete**. Engineering Fracture Mechanics, 74(4), 578-94.
10. Mazzotti, C., Savoia, M. and Ferracuti, B. (2008). **An experimental study on delamination of FRP plates bonded to concrete**. Construction and Building Materials, 22(7), 1409-21.
11. Chen, J. and Teng, J. (2001). **Anchorage Strength Models for FRP and Steel Plates Bonded to Concrete**. Journal of Structural Engineering, 127(7), 784-91.

12. De Lorenzis, L., Miller, B. and Nanni, A. (2001). **Bond of FRP laminates to concrete**. ACI Materials Journal, 98(3), 256-64.

13. Dai, J., Ueda, T. and Sato, Y. (2006). **Unified Analytical Approaches for Determining Shear Bond Characteristics of FRP-Concrete Interfaces through Pull-out Tests**. Journal of Advanced Concrete Technology, 4(1), 133-45.

14. Mitsui, M. Fukuzawa, K. Numao, T. Fuda, I (2000). **Relations between Surface Roughness Indexes and Bond Strength between CFRP Sheets and Concrete**. Journal of the Society of Materials Science, 49(6), 685-91.2.

15. Pan, J. and Leung, C. K. Y., **Effect of Concrete Composition on FRP/Concrete Bond Capacity**. Journal of Composites for Construction, 11(6), 611-8 (2007).

16. Lytag UK, **Introduction to Lytag lightweight aggregate**. Technical manual- section 1, July 2011.

17. SCGSM Laboratory Sheet, **Chemical Properties of Lytag aggregates**. the State Company of Geological Survey and Mining, Baghdad, Iraq.

18. Weber UK, **High-performance carbon fibre sheet reinforcement for structural strengthening**. Technical Report, July (2008).

19. McSweeney, B.M., &Lopez. M.M. (2005). **FRP-Concrete Bond Behaviour. A parametric Study through Pull-Off Testing**. In C.K Shield & J.P. Busel (Eds). Proceeding of the 7th International Symposium FRP Reinforcement for Concrete Structures, Kansas City, Missouri (PP.441-460).

20. Yao, J., Teng, J. G. and Chen, J. F. (2005). "**Experimental study on FRP-to-concrete bonded Joints**." Composites Part B: Engineering, 36(2), 99-113.

21. Woo, S. and Lee, Y. (2010). "**Experimental Study on Interfacial Behavior of CFRP-Bonded Concrete"** KSCE Journal of Civil Engineering, 4(3):385-393.

22. Martian, B., and Pantazopoulou, S.J. (2001). "**Effect of bond, aggregate interlock and dowel action on the shear strength degradation of reinforced concrete**." Engineering Structures 23, 214–227.

23. De Lorenzis, L., Miller, B. and Nanni, A. (2001). **Bond of FRP laminates to concrete**. ACI Materials Journal, 98(3), 256-64.

24. Xia, S. H. and Teng, J. G. (2005). **Behaviour of FRP-to-concrete bonded joints**. Proceedings of the International Symposium on Bond Behaviour of FRP in Structures (BBFS 2005), Hong Kong, 411-8.

25. FIB 14. **Externally bonded FRP reinforcement for RC structures**. International Federation for Structural Concrete – Technical report. Lausanne; 2001.

26. The Concrete Society, "**Design Guidance for Strengthening Concrete Structures Using Fibre Composites Materials**," Concrete Society, CS-TR-55-UK, Technical Report No. 55, third edition., Report of a Concrete Society Committee, Eynsham, UK, 2013.

27. Seracino R, Raizal Saifulnaz MR, Ohlers DJ (2007). **Generic debonding resistance of EB and NSM plate-to-concrete joints**. Journal of Composites for Construction, 11(1), 62–70.

28. Serbescu, A, Guadagnini, M., & Pilakoutas (2013). **Standardised double-shear test for determining bond of FRP to concrete and corresponding model development**. Composites Part B Engineering, 55, 277-279.